J. Micromech. Microeng. **16** (2006) 2044–2052 doi:10.1088/0960-1317/16/10/017

Modelling and control of an electrostatically actuated torsional micromirror

Guchuan Zhu[1], Muthukumaran Packirisamy[2], Mehran Hosseini[3] and Yves-Alain Peter[3]

[1] Department of Electrical Engineering, École Polytechnique de Montréal, C.P. 6079, Succursale centre-ville, Montreal, QC H3C 3A7, Canada
[2] Department of Mechanical and Industrial Engineering, Concordia University, 1455 de Maisonneuve Blvd. West, Montreal, QC H3G 1M8, Canada
[3] Engineering Physics Department, École Polytechnique de Montréal, C.P. 6079, Succursale centre-ville, Montreal, QC H3C 3A7, Canada

E-mail: guchuan.zhu@polymtl.ca

Received 7 June 2006
Published 25 August 2006
Online at stacks.iop.org/JMM/16/2044

Abstract
This work aims at developing control algorithms for an electrostatically actuated torsional micromirror, extending the operational range of the device to a full 90° tilt angle. The analytical model of the micromirror equipped with an additional vertical electrode is established. Since the geometrical extent of the device is comparable to the air gap, the effect of the fringing field is also incorporated into the model. It is shown that the considered system is differentially flat and, based on this property, a closed-loop control scheme is constructed for both scanning control and set-point control. In addition, the desired performance can be specified through reference trajectories, allowing the control system tuning to be performed in a systematic way. The simulation results demonstrate the advantage of the developed control scheme over the constant voltage control.

(Some figures in this article are in colour only in the electronic version)

1. Introduction

With its increased reliability and decreased manufacturing cost, the technology of microelectromechanical systems (MEMS) has been leveraged to benefit many industries, such as medicine, telecommunications, automotive and aerospace. Micromirror is one of the most widely used microoptoelectromechanical systems (MOEMS) devices. Among its many interesting applications, examples include laser printing, bar code reading, laser surgery and fine pointing mechanisms for inter- and intra-satellite laser communication systems, to name only a few.

Among the numerous approaches for actuating micro devices, for example, piezoelectric, thermopneumatic, electromagnetic and electrostatic forces, electrostatic actuation remains the most frequently applied principle in view of versatility and simple implementation [1]. However, when a static control scheme is used, the stable operational range of parallel-plate electrostatic actuators is limited by the *pull-in* phenomenon, which occurs when the rate of increase of the electrostatic torque becomes larger than that of the mechanical restoring torque at the equilibrium point. Beyond the pull-in position, the moveable electrode will suddenly and catastrophically snap down to the fixed one. There is an abundant literature relating to this topic (see, e.g., [2–9]). In some applications, e.g., torsional micromirrors, the continuous actuation range of the device may also be limited by the maximum capacitance of the device. When the capacitance of the actuator reaches its maximum value, the micromirror cannot move further as the force direction will reverse and this will limit the maximum angle of tilt of the micromirror.

Besides the pull-in instability issue, many applications of MEMS also impose stringent requirements on the actuator transient behaviour, such as, settling time, overshoot and oscillations. It is easy to illustrate that an over-damped system

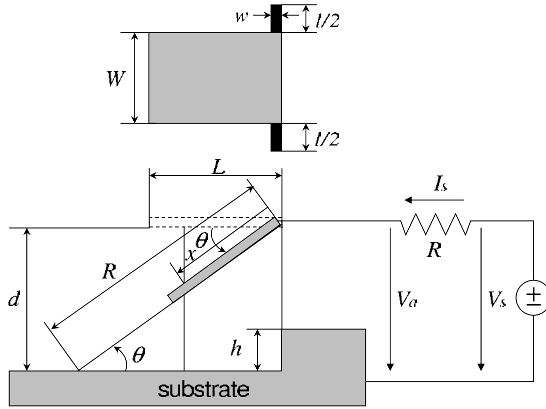

Figure 1. Scheme of a torsional micromirror.

will suffer from a long settling time, while an under-damped one will suffer from oscillations and overshoot. Note that when the moveable and fixed electrodes are close to each other, the overshoot will drive the moveable electrode to hit the fixed one. The unexpected contact could damage the surface of the electrodes and consequently reduce the lifetime of the device.

This paper addresses the modelling and control of an electrostatically actuated torsional mirror including an additional vertical electrode, allowing the device to attain a full 90° tilt angle. Such devices are demonstrated in, e.g., [10, 11]. The present work concentrates on the modelling and control of this type of actuator. More precisely, we first extend the modelling presented in [11], which provides a more accurate description of the capacitance of the device with respect to the deflection angle. Since the geometric extent of the device is comparable to the air gap, the effect of the fringing field is also considered in the modelling. Then we develop a nonlinear control scheme, allowing us to extend the stable actuation range to the full 90° range. The proposed control scheme is based on an essential geometric property of the system, namely differential flatness [12, 13], and it combines techniques of trajectory planning and feedback linearization control. It is therefore suited for both open-loop and closed-loop control, depending on application cases. Note that due to space limitation, we will not address the fabrication process of the device. Interested readers are referred to [10, 11] and references therein.

The rest of this paper is organized as follows. Section 2 establishes the model of a one degree of freedom (1DOF) torsional micromirror. Section 3 gives the dynamical model of the device and performs pull-in and stress analysis. Section 4 is devoted to control system design. The simulation results are reported in section 5. Finally, section 6 contains some concluding remarks.

2. Capacitance of 1DOF torsional micromirrors

The considered device in this work is a typical 90° scanning micromirror whose schematic representation is given in figure 1. The micromirror is sustained by torsional beams clamped at the ends as shown. The substrate acts as the fixed electrode and the micromirror is the moving electrode. The geometrical parameters of the device that were used for the present analysis are given in table 1. One should note that the dimensions of the mirror are in the range of a few hundred micrometres.

Table 1. Parameters of the electrostatic scanning micromirror.

Parameter	Value
Mirror width W	600 (μm)
Mirror length L	300 (μm)
Height of vertical electrodes h	60 (μm)
Air gap d	305 (μm)
Torsion beam width w	16 (μm)
Torsion beam length l	320 (μm)
Mirror and torsion beam thickness δ	0.4 (μm)
Permittivity ε	8.85×10^{-12} (F m^{-1})
Modulus of rigidity G	73 (GPa)

The device is actuated by a voltage source, where I_s, V_s and V_a are the source current, the applied voltage and the actuation voltage, respectively. The force created due to the electrostatic field between the mirror and the substrate will tilt the micromirror towards the substrate. The tilting will also give rise to a counter mechanical resisting torque from the torsional beams supporting the micromirror. In its tilted state, the mirror can effectively reflect the light in the desired direction.

Note that a vertical electrode, served also as a stopper, is added on the substrate, in order to increase the force due to its electrostatic field helping the micromirror to attend a 90° tilt angle [10, 11]. By this way, it is possible to tilt the mirrors to any desired angle using an appropriate control signal.

One of the most often used formulae for capacitance due to the horizontal electrode of the torsion microstructure is of the following form (see, e.g., [5]):

$$C_{\mathrm{hm}} = \frac{\varepsilon W}{\theta} \ln\left(\frac{d}{d - L\theta}\right), \tag{1}$$

where ε is the permittivity in the air gap. An equivalent model expressed as the electrical torque is given by [14]. This model takes into account only the main electrical field and is subjected to small tilt angles. In [11], this model is modified to take account of the capacitance due to the counter electric field. The modelling of a similar device can also be found in [10]. The formulation used in the above-mentioned work is still based on the assumption of small angular deflections and may not be accurate for large tilt angles.

From figure 1 it is easy to see that the capacitance due to the horizontal electrode can be extended to the full deflection range by replacing the term $d - L\theta$ with the actual vertical deflection of the moving plate, $d - L\sin\theta$, which yields

$$C_{\mathrm{hm}} = \frac{\varepsilon W}{\theta} \ln\left(\frac{d}{d - L\sin\theta}\right). \tag{2}$$

In addition, for structures of which the gap separating the two plates is comparable to the geometric extent, the effect of the fringing field is no longer negligible (see, e.g., [15]). Figure 2(*a*) shows the capacitance calculated by (1) and the results obtained by numerical simulation using MEMS CAD tool ConventorWare. It can be seen that for the considered device, the actual capacitance is much higher than the one that considered only the main field.

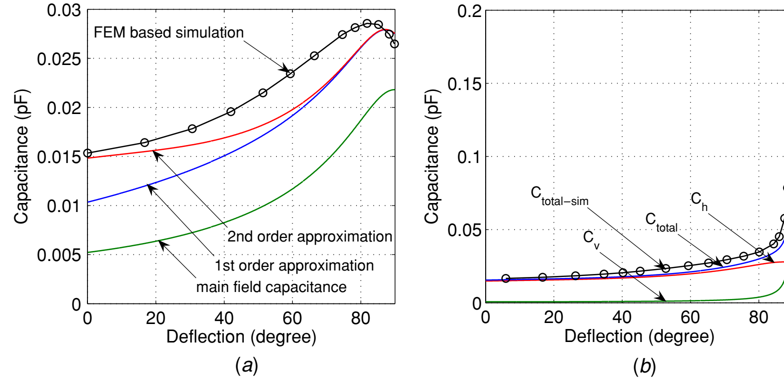

Figure 2. Capacitances for different modelling: (*a*) capacitance due to the horizontal electrode, (*b*) capacitance of the device.

To obtain a more accurate model that takes account of fringing capacitance, we start with the structure of microstrapline of width much smaller than length, $W \ll L$. The capacitance of such devices, including the effect of the fringing field, is given by [16]

$$C_{\mathrm{p}} = \frac{\varepsilon A}{x}\left(1 + \frac{2x}{\pi W} + \frac{2x}{\pi W}\ln\left(\frac{\pi W}{x}\right)\right), \tag{3}$$

where x is the air gap between the electrodes and A is the area of the electrode. This formulation can be extended to devices with an arbitrary shape by replacing W with the effective width [17]. For rectangular devices, the effective length is $L_{\mathrm{eff}} = 2L$. Therefore, the effective width is given by $W_{\mathrm{eff}} = A/L_{\mathrm{eff}} = W/2$. A modified expression of the capacitance can then be given by

$$C_{\mathrm{h}} = C_{\mathrm{hm}}\left(1 + \frac{2d}{\pi W_{\mathrm{eff}}} + \frac{2d}{\pi W_{\mathrm{eff}}}\ln\left(\frac{\pi W_{\mathrm{eff}}}{d}\right)\right), \tag{4}$$

where C_{hm} is the capacitance due to the main electrical field given by (1). The simulation result shows that the fringing capacitance is still underestimated (see figure 2(*a*)). It is reported in the literature that the first-order approximations of the form (3) often result in underestimated capacitances (see, e.g., [15]).

To further reduce the modelling error, we adapted the formulation of a second-order approximation proposed in [15] to torsion devices and yield

$$C_{\mathrm{h}} = C_{\mathrm{hm}}\gamma(\theta) \tag{5}$$

with

$$\gamma(\theta) = 1 + \frac{2d}{\pi W_{\mathrm{eff}}}\left(1 + \ln\left(\frac{\pi W_{\mathrm{eff}}}{d}\right)\right) + \left(\frac{d - L\sin\theta}{\pi W_{\mathrm{eff}}}\ln\left(\frac{d - L\sin\theta}{4\pi W_{\mathrm{eff}}}\right)\right)^2. \tag{6}$$

The capacitance given by the last expression is depicted in figure 2(*a*) and it can be seen that the modelling error is considerably reduced compared to the model deduced from the main field. Even though further improvement of modelling accuracy is possible, this will increase the complexity of the model and, consequently, make the implementation of control algorithms difficult.

Usually, the height of the stopper, h, is much smaller than the air gap, d, the capacitance due to the vertical electrode is then given by

$$C_{\mathrm{v}} = \varepsilon W\int_{d-h}^{L}\frac{\mathrm{d}x}{x\cos\theta} = \varepsilon W\ln\left(\frac{L}{d-h}\right)\frac{1}{\cos\theta}. \tag{7}$$

Hence, the total capacitance of the device is

$$C = C_{\mathrm{h}} + C_{\mathrm{v}} = C_0 C_\theta, \tag{8}$$

where

$$C_0 = \frac{\varepsilon W L}{d} \tag{9}$$

is the main field capacitance at the zero voltage position. Figure 2(*b*) shows the total capacitance calculated from (8) (C_{total}) and that obtained by numerical simulation with ConventorWare ($C_{\mathrm{total\text{-}sim}}$). We can see that the analytical model has a very good agreement with the simulation result.

3. Dynamical model and pull-in analysis

The equation of motion of the device is given by

$$J\ddot{\theta} + b\dot{\theta} + k\theta = T_{\mathrm{e}}, \tag{10}$$

where J is the mass moment of inertia of the moving electrode and b is the linear viscous damping coefficient. The restoring mechanical torque of torsion beams is supposed to be proportional to the tilt angle:

$$T_m = k\theta, \tag{11}$$

therefore the mechanical stiffness coefficient, k, is given as (see, e.g., [18])

$$k = \frac{2Gw\delta^3}{3l}\left(1 - \frac{192}{\pi^5}\frac{\delta}{w}\tanh\left(\frac{\pi w}{2\delta}\right)\right), \tag{12}$$

where G is the modulus of rigidity and the geometric dimension of torsion beams (w, l and δ) is defined in table 1.

The electrostatic torque can be obtained from the derivative of the capacitance with respect to the angular deflection which reads

$$T_{\mathrm{e}} = \frac{1}{2}V_a^2 C_0\frac{\partial C_\theta}{\partial\theta} = \frac{1}{2}V_a^2 C_0 C'_\theta, \tag{13}$$

where $C'_\theta = \partial C/\partial\theta$ is a function of θ. Figure 3 illustrates the effect of adding a vertical electrode for obtaining tilt angles

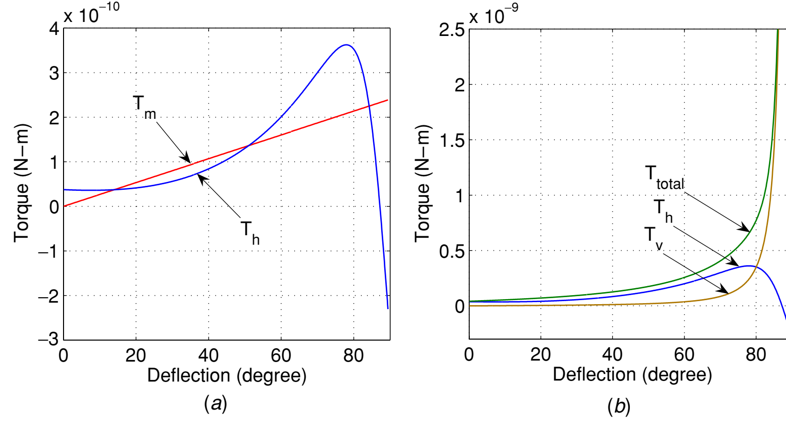

Figure 3. Electrostatic and mechanical torques: (*a*) mechanical torque of torsion beams and electrostatic torque due to the horizontal electrode for $V_a = 150$ (V), (*b*) electrostatic torques for $V_a = 150$ (V).

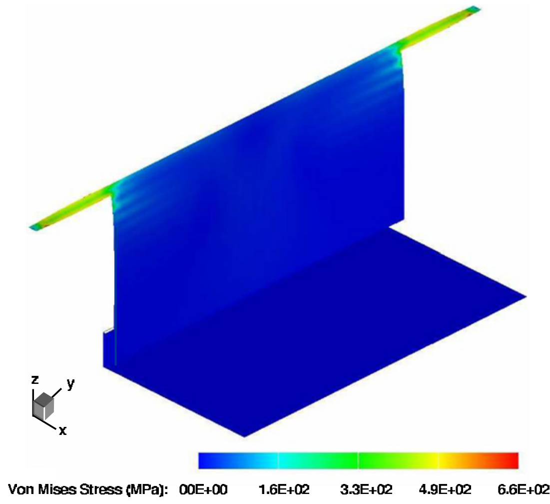

Figure 4. CoventorWare simulation of stress distribution for 88.4° deflection.

from 0° to 90°. The electrostatic torques are obtained for a voltage $V_a = 150$ (V) and are expressed as the functions of deflection. It can be seen from figure 3(*a*) that in the absence of the vertical electrode, there are three equilibria in the operation range. Due to the fact that when the capacitance of the actuator reaches its maximum value, the force direction will be reversed, the micromirror is unable to attend a full 90° tilt. Adding a vertical electrode of sufficient height will render the capacitance and the electrostatic torque monotonic (see figures 2(*b*) and 3(*b*)), allowing the device to achieve a full 90° tilt angle actuation.

Even though the dynamical model of the device depends only on its geometry, it is necessary to verify the maximum stress to assure a safe operation. CoventorWare has been used to simulate the stress distribution of the device under investigation for a deflection near 90° and the result is shown in figure 4. It can be seen that the maximum von Mises stress is about 660 MPa, which is much lower than the typical yield strength of silicon (7 GPa) [19]. Therefore, the device can safely operate in the whole range of deflection.

It has been shown that for actuators with one degree of freedom, the pull-in angle is only related to the geometry of the device and does not depend on spring structures. Furthermore, the pull-in angle can be obtained by solving the following equation (see, e.g., [7]):

Table 2. Pull-in angles and pull-in voltages corresponding to different stopper heights.

Stopper height (μm)	Pull-in angle (°)	Pull-in voltage (V)
20	28.09	213.29
30	27.87	208.23
40	27.65	203.34
50	27.43	198.61
60	27.21	194.03

$$\left.\frac{\partial C}{\partial \theta}\right|_{\theta=\theta_{\rm pi}} - \theta_{\rm pi} \left.\frac{\partial^2 C}{\partial \theta^2}\right|_{\theta=\theta_{\rm pi}} = 0, \tag{14}$$

and the pull-in voltage is given by

$$V_{\rm pi} = \sqrt{\frac{2k}{\left.\frac{\partial^2 C}{\partial \theta^2}\right|_{\theta=\theta_{\rm pi}}}} = \sqrt{\frac{2k}{C''_{\theta_{\rm pi}}}} = \sqrt{\frac{2k\theta_{\rm pi}}{C'_{\theta_{\rm pi}}}}, \tag{15}$$

where $C''_\theta = \partial^2 C/\partial\theta^2$ and $\theta_{\rm pi}$ indicate the pull-in angle. By numerically solving equation (14), we got the pull-in angle and the corresponding pull-in voltage for different stopper heights, as shown in table 2.

It now remains to model the dynamics of the driven circuit as shown in figure 1. Assuming that the system started operating from an initially uncharged state at $t = 0$, then the charge in the electrodes at the time t is

$$Q(t) = \int_0^t I_s(\tau)\,\mathrm{d}\tau, \tag{16}$$

or equivalently

$$\dot{Q}(t) = I_s(t). \tag{17}$$

Since the voltage across the plates $V_a = Q(t)/C_t(t)$, the current through the resistor R can be obtained by a simple application of Kirchhoff's voltage law as [20]

$$\dot{Q}(t) = \frac{1}{R}\left(V_s(t) - \frac{Q(t)}{C_t(t)}\right). \tag{18}$$

Note that

$$V_a^2 C_0 C'_\theta = \frac{1}{C_0}\frac{C'_\theta Q^2}{C_\theta^2}.$$

Therefore by denoting

$$\alpha_\theta = \frac{C'_\theta}{C_\theta^2}, \tag{19}$$

the electrostatic torque T_e can be expressed as

$$T_e = \frac{1}{2C_0}\alpha_\theta Q^2. \tag{20}$$

To make the system analysis and control design easier, the system (10)–(18) is transformed into normalized coordinates by changing the time scale, $\tau = \omega_n t$, and performing a normalization as follows:

$$q = \beta\frac{Q}{Q_{pi}}, \qquad u = \beta\frac{V_s}{V_{pi}}, \qquad i = \frac{I_s}{V_{pi}\omega_n C_0}, \qquad r = \omega_n C_0 R, \tag{21}$$

where $Q_{pi} = C_0 V_{pi}$ is the pull-in charge corresponding to the pull-in voltage, $\omega_n = \sqrt{k/J}$ is the undamped natural frequency, $\zeta = b/2J\omega_n$ is the damping ratio and $\beta = \sqrt{C_0/C''_\theta(\theta_{pi})}$.

Let $\omega = \dot\theta$ be the angular velocity of the moveable electrode, then the system (10) and (18) can be written in the normalized coordinates as

$$\begin{cases} \dot\theta = \omega \\ \dot\omega = -2\zeta\omega - \theta + \alpha_\theta q^2 \\ \dot q = -\dfrac{q}{rC_\theta} + \dfrac{1}{r}u, \end{cases} \tag{22}$$

which is defined in state space $\mathcal{X} = \{(\theta, \omega, q) \subset \mathbb{R}^3 \mid \theta \in [0, \pi/2]\}$.

Finally, in the following study, the tilt angle of the micromirror is considered as the output of the system

$$y = \theta. \tag{23}$$

Since the system analysis and control design will be performed in the normalized coordinates, we can use t to denote the time and omit the qualifier 'normalized', if no confusion will be introduced.

4. Flatness-based control of torsional micromirrors

4.1. Differential flatness and trajectory planning

In order to deduce the control law, we compute the time derivatives of the output until that the input appears and we obtain

$$\begin{aligned} \dot y &= \omega, \\ \ddot y &= \dot\omega = -2\zeta\omega - \theta + \alpha_\theta q^2, \\ y^{(3)} &= -2\zeta\dot\omega - \dot\theta + \dot\alpha_\theta q^2 + 2\alpha_\theta q\dot q \\ &= -2\zeta\ddot y - (1 - \alpha'_\theta q^2)\dot y + 2\alpha_\theta q\left(-\frac{q}{rC_\theta} + \frac{1}{r}u\right), \end{aligned}$$

where $\alpha'_\theta = \partial\alpha_\theta/\partial\theta$ is clearly a function of θ and hence, a function of the output. Note that the length of integration channel from the input to the output is exactly the dimension of the dynamical model. Furthermore, all the state variables, as well as the input can be explicitly expressed as functions of the output y and its derivatives $\dot y$, $\ddot y$ and $y^{(3)}$, and are given as

$$\theta = y, \tag{24}$$

$$\omega = \dot y, \tag{25}$$

$$q = \sqrt{\frac{\ddot y + 2\zeta\dot y + y}{\alpha_\theta(y)}}, \tag{26}$$

$$u = \frac{r}{2\alpha_\theta(y)q}(y^{(3)} + 2\zeta\ddot y + \dot y) - q\left(\frac{r\alpha'_\theta(y)}{\alpha_\theta(y)}\dot y - \frac{1}{C_\theta(y)}\right). \tag{27}$$

Therefore system (22) is said to be differentially flat with $y = \theta$ as flat output [12, 13].

One of the basic properties of flat systems is that they are linearizable by a (dynamic) state feedback. In fact, it can be seen from (27) that

$$u = \frac{r}{2\alpha_\theta(y)q}(v + 2\zeta\ddot y + \dot y) - q\left(\frac{r\alpha'_\theta(y)}{\alpha_\theta(y)}\dot y - \frac{1}{C_\theta(y)}\right) \tag{28}$$

is a linearizing feedback control law that, with a diffeomorphism, renders system (22) into the Brunovsky canonical form

$$y^{(3)} = v \tag{29}$$

in the new coordinates, which is obviously linear with v as its input.

Another important feature of flat systems is that it is possible to compute any trajectory of the system without integrating the corresponding differential equations. This makes the trajectory planning simple and straightforward, as control signals can easily be deduced from the desired outputs, allowing the system to track arbitrary trajectories, up to some conditions of smoothness and feasibility. This property can also be used to construct control laws and it will be seen that the micromirror can operate beyond the pull-in position.

Note that reference trajectories can be expressed by any suitable function. To steer the system from an initial point x_i in state space at time t_i to a desired point x_f in state space at time t_f, one only needs to find a sufficiently smooth trajectory $t \mapsto y_r(t)$, such that the initial and final conditions are verified. Since the trajectory $t \mapsto y_r(t)$ does not need to verify any differential equations, it can be simply constructed, for example, by polynomial interpolations [21]. To illustrate the construction of trajectories, we consider a single-input/single-output (SISO) system. Extending the algorithm to multiple-input/multiple-output (MIMO) systems will be straightforward. Consider at time t_i,

$$y(t_i), \ldots, y^{(r+1)}(t_i)$$

and at time t_f,

$$y(t_f), \ldots, y^{(r+1)}(t_f)$$

are known and they define a total of $2(r+2)$ conditions for the output $y_r(t)$. Denote $T = t_f - t_i$ and $\tau(t) = (t - t_i)/T$, $y_r(t)$ can then be expressed as a polynomial of time of order equal to $2r + 3$:

$$y_r(t) = \sum_{k=0}^{2r+3} a_k\tau^k(t). \tag{30}$$

By deriving $y_r(t)$ $(r + 1)$-times and imposing the initial conditions, the first $r + 2$ coefficients $a_0, \ldots, a_{r+1}$ are given by

$$a_k = \frac{T^k}{k!}y^{(k)}(t_i), \qquad k = 0, \ldots, r + 1. \tag{31}$$

While the rest $r+2$ coefficients can be determined by the initial and final conditions, and are given by

$$\begin{pmatrix} 1 & 1 & \cdots & 1 \\ r+2 & r+3 & \cdots & 2r+3 \\ (r+1)(r+2) & (r+2)(r+3) & \cdots & (2r+2)(2r+3) \\ \vdots & \vdots & \cdots & \vdots \\ (r+2)! & \dfrac{(r+3)!}{2} & \cdots & \dfrac{(2r+3)!}{(2r+2)} \end{pmatrix} \times \begin{pmatrix} a_{r+2} \\ \vdots \\ \vdots \\ a_{2r+3} \end{pmatrix} = \begin{pmatrix} y(t_f) - \sum_{l=0}^{r+1} \frac{T^l}{l!} y^{(l)}(t_i) \\ \vdots \\ T^k \left(y^{(k)}(t_f) - \sum_{l=k}^{r+1} \frac{T^{l-k}}{(l-k)!} y^{(l)}(t_i) \right) \\ \vdots \\ T^{r+1} \left(y^{(r+1)}(t_f) - y^{(r+1)}(t_i) \right) \end{pmatrix}. \tag{32}$$

The technique of trajectory planning can also be applied to stabilize the system around setpoints. In this case, the reference trajectory will connect two equilibrium points. It results consequently that the derivatives of the reference trajectory should vanish at the initial and final positions, $y(t_i)$ and $y(t_f)$, and hence, the planned trajectory becomes

$$y_r(t) = y(t_i) + (y(t_f) - y(t_i))\tau^{r+2}(t) \sum_{k=0}^{r+1} a_k \tau^k(t), \tag{33}$$

where the coefficients $a_0, \ldots, a_{r+1}$ can be obtained by solving the following linear equation system:

$$\begin{pmatrix} 1 & 1 & \cdots & 1 \\ r+2 & r+3 & \cdots & 2r+3 \\ (r+1)(r+2) & (r+2)(r+3) & \cdots & (2r+2)(2r+3) \\ \vdots & \vdots & \cdots & \vdots \\ (r+2)! & \dfrac{(r+3)!}{2} & \cdots & \dfrac{(2r+3)!}{(2r+2)} \end{pmatrix} \times \begin{pmatrix} a_0 \\ a_1 \\ \vdots \\ a_{r+1} \end{pmatrix} = \begin{pmatrix} 1 \\ 0 \\ \vdots \\ 0 \end{pmatrix}. \tag{34}$$

As all the time derivatives of $y(t)$ vanish at the equilibria, the desired trajectory can be represented by a polynomial of arbitrary finite order. This allows the addition of more degrees of freedom in tuning the trajectory and obtaining the desired behaviour (e.g. fast rise time, low overshoot and well-damped oscillations).

For the micromirror under investigation, we can consider

$$\dot{y}_i = \dot{y}_f = 0, \qquad \ddot{y}_i = \ddot{y}_f = 0, \qquad y_i^{(3)} = y_f^{(3)} = 0.$$

The desired trajectory $t \mapsto y(t)$ is then of the following form:

$$y_r(t) = y_i + (y_f - y_i)\tau^5(t) \sum_{i=0}^{4} a_i \tau^i(t). \tag{35}$$

The coefficients in (35) can be obtained by solving (34) and are given as $a_0 = 126$, $a_1 = -420$, $a_2 = 540$, $a_3 = -315$ and $a_4 = 70$.

4.2. Closed-loop control

In an open-loop control scheme, the control signals are computed on the basis of the model of system dynamics. Clearly, if the model is perfectly known and environmental disturbances are negligible, the output of the system should follow the planned one. However, in the presence of system modelling error, parameter variations and external perturbations, the output of the system, in general, will not coincide with or even may diverge from the reference trajectory. A closed-loop control driven by instantaneous measurements of entire or partial state of the system will render the system more robust and help tracking reference trajectories.

Being differentially flat, the tracking problem of micromirror can be solved through the linearized system under the form of (29). Let $y_r(t)$ be the desired trajectory, and $e = y - y_r$ be the tracking error. A closed-loop control corresponding to system (29) can be chosen as

$$v = y_r^{(3)} - k_2(\ddot{y} - \ddot{y}_r) - k_1(\dot{y} - \dot{y}_r) - k_0(y - y_r). \tag{36}$$

Then, the tracking error e satisfies

$$e^{(3)} + k_2\ddot{e} + k_1\dot{e} + k_0 e = 0 \tag{37}$$

and will be exponentially stable around the origin if the characteristic equation

$$p(s) = s^3 + k_2 s^2 + k_1 s + k_0 \tag{38}$$

is Hurwitz stable. Consequently, u given by (28) will be a feedback control law archiving a local exponential tracking of the reference trajectory.

Usually, the controller gains in (36), k_0, k_1 and k_2, are determined from the performance requirement. However, it is often not evident how the performance specified in the linearized coordinates will affect that in the original coordinates. In the absence of any specific consideration, controller parameters can be chosen in a way that the location of closed-loop poles satisfies the Butterworth configuration. The control is thus optimal in the sense that as control effort becomes increasingly less expensive, the closed-loop poles should tend to radiate out from the origin along the spokes of a wheel in the left half-plane [22] as given by the roots of

$$\left(\frac{s}{\Omega}\right)^{2k} = (-1)^{k+1}, \tag{39}$$

where k is the number of poles in the left half-plane and Ω is the radius of the cycle on which the poles are placed. For example, the third-order Butterworth polynomial $B_3(z)$, $z = s/\Omega$, is of the form

$$B_3(z) = z^3 + 2z^2 + 2z + 1, \tag{40}$$

and the corresponding pole location is shown in figure 5.

Now controller gains become

$$k_0 = \Omega^3, \qquad k_1 = 2\Omega^2, \qquad k_2 = 2\Omega,$$

and Ω is the only tuning parameter, whose value can be chosen on the basis of desired decay rate and control effort.

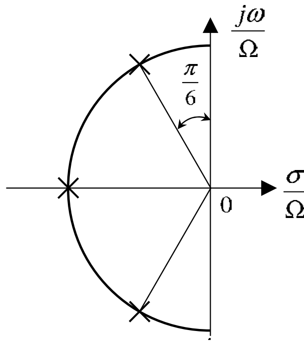

Figure 5. Pole replacement of the third-order Butterworth polynomial.

4.3. Speed observer design

Usually, the charge on the device and the angular deflection can be deduced from the input current, the voltage across the device and the capacitance. However, directly sensing the angular velocity during the normal operation of the device is extremely difficult, if not impossible. Therefore we need to construct a speed observer in order to provide the estimate of ω required for implementing the closed-loop control schemes described previously. A reduced-order speed observer can be constructed as follows. Let

$$z = \omega - k_\omega \theta, \tag{41}$$

where k_ω is an arbitrary positive real number. Differentiating (41) and using (22), we get

$$\dot{z} = -((2\zeta + k_\omega)k_\omega + 1)\theta - (2\zeta + k_\omega)z + \alpha(\theta)q^2. \tag{42}$$

Thus, if we set

$$\hat{z} = \hat{\omega} - k_\omega \theta,$$

where $\hat{\omega}$ is the required estimate of ω and $\hat{z}$ is the estimate of z, then

$$\dot{\hat{z}} = -((2\zeta + k_\omega)k_\omega + 1)\theta - (2\zeta + k_\omega)\hat{z} + \alpha(\theta)q^2. \tag{43}$$

Letting $e = \hat{z} - z = \hat{\omega} - \omega$ the estimation error, and $\frac{d}{dt}(\hat{z} - z) = \frac{d}{dt}(\hat{\omega} - \omega) = \dot{e}$, the error dynamics can be deduced from (42) and (43) as

$$\dot{e} = -(2\zeta + k_\omega)e, \tag{44}$$

which is globally exponentially stable at the origin with a decay rate defined by k_ω. This implies that

$$\hat{\omega} = \hat{z} + k_\omega \theta \tag{45}$$

and (43) forms an exponential observer.

5. Simulation results

In the following, we use the numerical simulation to verify the performance of the proposed control algorithm. Two cases will be dealt in simulation studies: scanning control and set-point control. The parameters of the considered micromirror are [11]

$$\zeta = 0.164, \qquad \omega_n = 5.7681 \times 10^3 \text{ (rad s}^{-1}\text{)},$$

and the stopper height is chosen to be 60 μm.

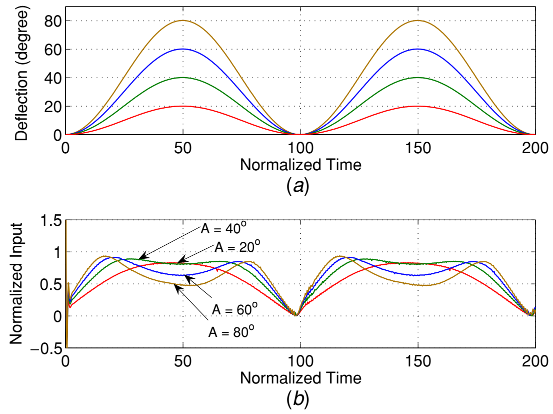

Figure 6. Responses of closed-loop scanning control for different scanning ranges: (*a*) system responses, (*b*) control signals.

5.1. Scanning control

Due to the nonlinearity associated with the micromirror, scanning controls deduced from the static relation between the position and actuation voltage would exhibit important distortions. In addition, such a control is limited by the pull-in angle, which is about 30° in our case (see table 2). In the simulation, the desired scanning curves are chosen as a sine wave form with a different scanning range A and normalized frequency $1/T_s$:

$$y_r(\tau) = \frac{A}{2}\left(1 + \sin\left(\frac{2\pi}{T_s}\tau + \frac{3}{2}\pi\right)\right), \tag{46}$$

where $\tau = \omega_0 t$ is the normalized time. Figure 6 shows the simulation results for scanning range A equal to 20°, 40°, 60° and 80°, and figure 7 shows the responses corresponding to different scanning periods, $T_s = 100, T_s = 50$ and $T_s = 25$. Clearly, the output of the system follows the reference trajectories quite well. We have observed that further increasing the scanning amplitude or frequency could cause instability. This is mainly due to the fact that those reference trajectories are not feasible. The control signals corresponding to different scanning curves are also shown. Obviously, the relationship between the input and output is highly nonlinear. Therefore, it will be extremely difficult to generate desired scanning curves using the method of static voltage inversion. Note that the nominal damping ratio used in the controller design is $\zeta = 1$, while its actual value is 0.164. This shows the robustness of the closed-loop control. We have observed that the performance of the system is not significantly affected by stopper height.

5.2. Set-point control

For set-point control, we tested the deflection of 10°, 45° and 89°. The reason to choose 89° as a test case is to show that the system is indeed stable near a 90° deflection. The travelling time from $y_r(t_i)$ to $y_r(t_f)$ is set to 10 (normalized time units), or about 3 ms in the original timescale. We can see from figure 8 that the closed-loop set-point control scheme allows a full 90° operation and provides an excellent performance, even in the presence of system parameter uncertainty (mismatch of damping ratio).

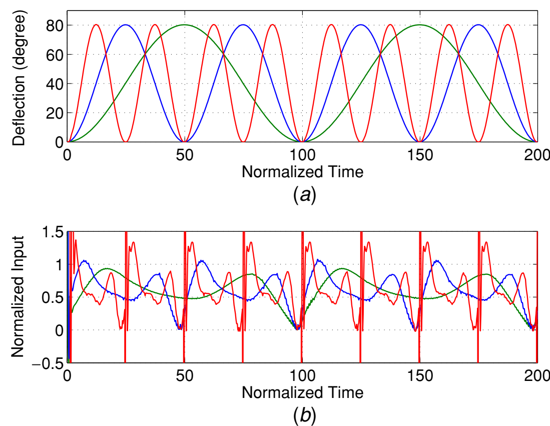

Figure 7. Responses of closed-loop scanning control for different scanning periods: (*a*) system responses, (*b*) control signals.

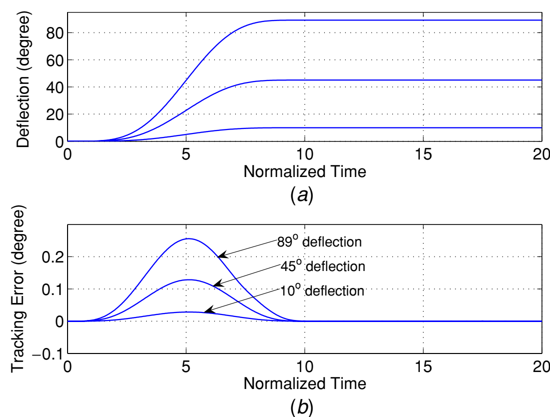

Figure 8. Responses of closed-loop set-point control: (*a*) system responses, (*b*) tracking errors.

Finally, note that the shorter the expected travelling time, the larger the effort that is required to control the device. Therefore, in practice, an appropriate compromise must be made in order to obtain a satisfactory performance while not using excessive control forces. Note also that further diminution of planned travelling time could render the reference trajectory infeasible and make the system unstable.

6. Concluding remarks

This paper addressed the modelling and control of a 1DOF torsional micromirror. A capacitance-based modelling of a micromirror is presented. This model incorporates capacitance due to different electrostatic fields into a single analytical expression and is indispensable for control system analysis and design. The effect of the fringing field is also considered. Note that the highly nonlinear capacitance given by (6) is still an approximative expression. In practice, more accurate expressions are very difficult to obtain and might render control algorithms extremely complicated. A possible solution for tackling this problem is to use robust control schemes.

It has been shown that electrostatically actuated 1DOF torsional micromirrors are differentially flat and, based on this property, a closed-loop control scheme has been constructed. The proposed control scheme allows us to extend the operational range to a full 90° tilt angle and improve the system performance in terms of transient response, precision and robustness.

Acknowledgments

This work was supported in part by the École Polytechnique de Montréal under a program of start-up funds. The authors gratefully acknowledge Professor Jean Lévine of the Centre Automatique et Systèmes of the École des Mines de Paris for pointing out the potential applications of flat system theory in the control of MEMS.

References

[1] Thielicke E and Obermeier E 2000 Microactuators and their technologies *Mechatronics* **10** 431–55
[2] Hornbeck L J 1989 Deformable-mirror spatial light modulators in *SPIE Crit. Rev. Ser.* **1150** 86–102
[3] Nemirovsky Y 1998 Pull-in study of an electrostatic torsion microactuator *IEEE J. Microelectromech. Syst.* **7** 373–9
[4] Degani O, Socher E, Lipson A, Leitner T, Setter D J, Kaldor S and Nemirovsky Y 1998 Pull-in study of an electrostatic torsion microactuator *J. Microelectromech. Syst.* **7** 373–9
[5] Xiao Z, Wu X, Peng W and Farmer K R 2001 An angle-based design approach for rectangular electrostatic torsion actuators *J. Microelectromech. Syst.* **10** 561–8
[6] Nemirovsky Y and Bochobza-Degani O 2001 A methodology and model for the pull-in parameters of electrostatic actuators *J. Microelectromech. Syst.* **10** 601–15
[7] Hah D, Toshiyoshi H and Wu M C 2002 Design of electrostatic actuators for MOEMS *Proc. Symp. on Design, Test, Integration and Packaging of MEMS/MOEMS (DTIP 2002) (Cannes-Mandelieu, France)* pp 200–07
[8] Bochobza-Degani O and Nemirovsky Y 2002 Modeling the pull-in parameters of electrostatic actuators with a novel lumped two degrees of freedom pull-in model *Sensors Actuators* A **97–98** 569–78
[9] Xiao Z, Peng W and Farmer K R 2003 Analytical behavior of rectangular electrostatic torsion actuators with nonlinear spring bending *J. Microelectromech. Syst.* **12** 929–36
[10] Yoon Y S, Kim J H, Choi H and Koh B C 2003 A low voltage actuated micromirror with an extra vertical electrode for 90° rotation *J. Micromech. Microeng.* **13** 922–6
[11] Bhaskar A K, Packirisamy M and Bhat R B 2004 Modeling switching response of torsional micromirrors for optical microsystems *J. Mech. Mach. Theory* **39** 1399–410
[12] Fliess M, Lévine J, Martin P and Rouchon P 1995 Flatness and defect of non-linear systems: introductory theory and examples *Int. J. Control* **61** 1327–61
[13] Fliess M, Lévine J, Martin P and Rouchon P 1999 A Lie–Bäcklund approach to equivalence and flatness of nonlinear systems *IEEE Trans. Autom. Control* **44** 922–37
[14] Toshiyoshi H and Fujita H 1996 Electrostatic micro torsion mirrors for an optical switch matrix *J. Microelectromech. Syst.* **5** 231–7
[15] Sloggett G J, Barton N G and Spencer S J 1986 Fringing fields in disc capacitors *J. Phys. A: Math. Gen.* **19** 27250–2736
[16] Kirchhoff G 1877 Zur theorie des kondensators *Mon. Akad. Wiss. Berl.* 101–20
[17] Steeneken P G, Rijks T G S M, van Beek J T M, Ulenaers M J E, de Coster J and Puers R 2005

Dynamics and squeeze film gas damping of a capacitive RF MEMS switch *J. Micromech. Microeng.* **15** 176–84

[18] Gere J M and Timoshenko S P 1997 *Mechanics of Materials* 4th edn (Boston: PWS)

[19] Petersen K E 1982 Silicon as a mechanical material *Proc. IEEE* **70** 420–57

[20] Senturia S D 2001 *Microsystem Design* (Norwell, MA: Kluwer)

[21] Lévine J 2004 *Analyse et Commande des Systèmes Non Linéaires* http://cas.ensmp.fr/%7Elevine/Enseignement/CoursENPC.pdf

[22] Friedland B 1986 *Control System Design: An Introduction to State-Space Methods* (New York: McGraw-Hill)